ChemPubSoc Europe

DOI: 10.1002/chem.201502720

CHEMISTRY A European Journal Full Paper

Single-Molecule Magnets

# Single-Molecule Magnetism, Enhanced Magnetocaloric Effect, and Toroidal Magnetic Moments in a Family of $Ln_4$ Squares

Chinmoy Das,[a] Shefali Vaidya,[a] Tulika Gupta,[a] Jamie M. Frost,[c] Mattia Righi,[b] Euan K. Brechin,[c] Marco Affronte,*[b] Gopalan Rajaraman,*[a] and Maheswaran Shanmugam*[a]

**Abstract:** Three cationic [$Ln_4$] squares (Ln = lanthanide) were isolated as single crystals and their structures solved as $[Dy_4(\mu_4\text{-}OH)(HL)(H_2L)_3(H_2O)_4]Cl_2\cdot(CH_3OH)_4\cdot(H_2O)_8$ (**1**), $[Tb_4(\mu_4\text{-}OH)(HL)(H_2L)_3(MeOH)_4]Cl_2\cdot(CH_3OH)_4\cdot(H_2O)_4$ (**2**) and $[Gd_4(\mu_4\text{-}OH)(HL)(H_2L)_3(H_2O)_2(MeOH)_2]Br_2\cdot(CH_3OH)_4\cdot(H_2O)_3$ (**3**). The structures are described as hydroxo-centered squares of lanthanide ions, with each edge of the square bridged by a doubly deprotonated $H_2L^{2-}$ ligand. Alternating current magnetic susceptibility measurements show frequency-dependent out-of-phase signals with two different thermally assisted relaxation processes for **1**, whereas no maxima in $\chi_M$" appears above 2.0 K for complex **2**. For **1**, the estimated effective energy barrier for these two relaxation processes is 29 and 100 K. Detailed ab initio studies reveal that complex **1** possesses a toroidal magnetic moment. The ab initio calculated anisotropies of the metal ions in complex **1** were employed to simulate the magnetic susceptibility by using the Lines model (POLY_ANISO) and this procedure yields $J_1 = +0.01$ and $J_2 = -0.01$ $cm^{-1}$ for **1** as the two distinct exchange interactions between the $Dy^{III}$ ions. Similar parameters are also obtained for complex **1** (and **2**) from specific heat measurements. A very weak antiferromagnetic super-exchange interaction ($J_1 = -0.043$ $cm^{-1}$ and $g = 1.99$) is observed between the metal centers in **3**. The magnetocaloric effect (MCE) was estimated by using field-dependent magnetization and temperature-dependent heat-capacity measurements. An excellent agreement is found for the $-\Delta S_m$ values extracted from these two measurements for all three complexes. As expected, **3** shows the largest $-\Delta S_m$ variation ($23\ J\,Kg^{-1}\,K^{-1}$) among the three complexes. The negligible magnetic anisotropy of Gd indeed ensures near degeneracy in the $(2S+1)$ ground state microstates, and the weak super-exchange interaction facilitates dense population of low-lying excited states, all of which are likely to contribute to the MCE, making complex **3** an attractive candidate for cryogenic refrigeration.

## Introduction

The large magnetic moments and unquenched first-order orbital angular momenta associated with certain lanthanide ions make their coordination complexes potentially useful in various applications, such as information storage,[1] spintronics,[2] molecular switches,[3] spin valves,[4] and qubits.[5] The academic investigation of the magnetic behavior of lanthanide-based molecular cages has been reinvigorated since the discovery of single-molecule-magnet (SMM) behavior in a mononuclear terbium phthalocyanine complex.[6] Following this, several lanthanide-based SMMs, in particular dysprosium-based clusters, ranging from monomers to tetracosanuclear species, have been reported.[1h,7] Among them, multinuclear clusters often show unusual magnetic properties. Fascinating recent examples include $Dy_3$ triangles in which the SMM behavior originates from the excited states,[8] $Dy_5$ and $Dy_4K_2$ clusters exhibiting enormous effective-energy-barrier ($U_{eff}$) values,[1b] and the presence of magnetic bistability in symmetric, oligomeric, lanthanide complexes as a result of a toroidal arrangement of anisotropic axes.[7b]

Although various promising synthetic approaches have been reported in efforts to increase the $U_{eff}$ value, the blocking temperature ($T_B$) associated with the onset of hysteresis in molecular systems still sits below $T = 14$ K,[9] hampering any realistic development of molecular devices for practical applications. This is partly due to the lack of understanding of the combined roles of orbital ($L$) and spin ($S$) angular momenta to the resultant magnetic moment of the molecule. Moreover, further complications may arise due to the varying contributions of $L$ and $S$ with different geometries around the lanthanide ions.[10] Molecular complexes constructed of metal ions with negligible

[a] C. Das, S. Vaidya, T. Gupta, Prof. Dr. G. Rajaraman, Prof. Dr. M. Shanmugam
Department of Chemistry, Indian Institute of Technology Bombay
Powai, Mumbai, Maharashtra, 400076 (India)
E-mail: eswar@chem.iitb.ac.in
rajaraman@chem.iitb.ac.in

[b] M. Righi, Prof. Dr. M. Affronte
CNR Institute of Nanosciences S3 and Dipartimento di Scienze Fisiche Infomatiche e Matematiche, Università di Modena e Reggio Emilia
via G. Campi213 A, 41125 Modena (Italy)
E-mail: marco.affronte@unimore.it

[c] J. M. Frost, Prof. Dr. E. K. Brechin
EaStCHEM School of Chemistry, The University of Edinburgh
David Brewster Road, Edinburgh, EH9 3FJ (UK)

Supporting information for this article is available on the WWW under http://dx.doi.org/10.1002/chem.201502720.

magnetic anisotropy, such as $Gd^{III}$, have been proposed for various applications, including contrast agents in magnetic resonance imaging,[11] spin-labeling,[12] dynamic nuclear polarization,[13] and cryogenic refrigeration, which takes advantage of the intrinsic magnetocaloric effect (MCE) of these materials.[14] Following the idea proposed by Shull and co-workers of employing nanoparticles for magnetic refrigeration,[15] a plethora of 0–3D molecule-based materials have been reported as promising candidates, particularly by Evangelisti and co-workers, who recently described certain molecular requirements, including the importance of a large magnetic density (i.e., the use of lightweight ligands), in achieving improved MCE efficiency, together with large *S*, weak *J*, and negligible *D*.[14e,16]

In this line of interest and to reveal a new generation of lanthanide based clusters with both isotropic and anisotropic lanthanide metal ions, we have employed the multidentate Schiff base ligand ($H_4L$, Scheme 1), for which the coordination potential has been previously investigated.[10a,17]

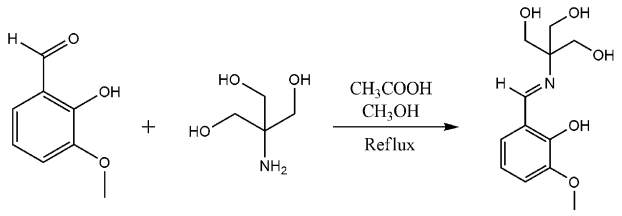


**Scheme 1.** Synthetic scheme followed to make $H_4L$. See the Experimental Section for full details.

In this article, we report three analogous $Ln^{III}_4$ squares of general formula $[Ln_4(\mu_4\text{-}OH)(HL)(H_2L)_3(Y)_4]X_2$ cluster (Ln = $Dy^{III}$, $Tb^{III}$, $Gd^{III}$; Y = solvent, X = halide). The structures were determined by single-crystal X-ray diffraction. The magnetothermal properties were investigated by variable-temperature, variable-field, susceptibility, magnetization and specific heat measurements. To further support our experimental findings, we performed CASSCF + RASSI-SO calculations. This detailed experimental and theoretical investigation reveals that complex **1** exhibits a rare toroidal magnetic moment, which is evident from the magnetization measurements, and complex **3** shows large variation in $-\Delta S_m$, making it a promising candidate for cryogenic refrigeration.

## Results and Discussion

The reaction between the Schiff base ligand $H_4L$ and a lanthanide halide ($DyCl_3{\cdot}6H_2O$, $TbCl_3{\cdot}6H_2O$ or $GdBr_3{\cdot}6H_2O$) in the presence of NaOMe in methanol results in the formation of pale yellow single crystals of complexes **1**–**3** after one week. X-ray diffraction reveals the structure to be $[Ln_4(\mu_4\text{-}OH)(HL)(H_2L)_3(Y)_4]X_2$ (where Ln = $Dy^{III}$, Y = $H_2O$, X = Cl (**1**); Ln = $Tb^{III}$, Y = MeOH, X = Cl (**2**); and Ln = $Gd^{III}$, Y = MeOH, X = Br (**3**)). The molecular structures of all three complexes are isomorphous, a representative structure is given in Figure 1, with individual structures in Figure S1 in the Supporting Information. The corresponding crystallographic data is listed in Table 1.

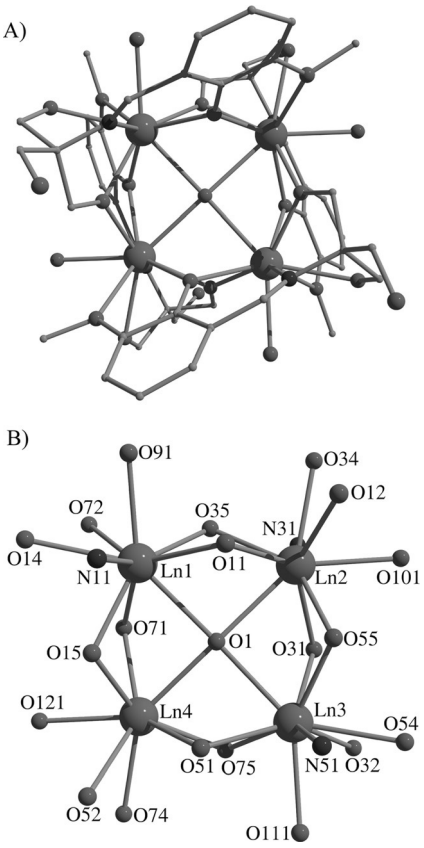


**Figure 1.** A) A representative crystal structure of the cationic complexes **1**–**3**. B) The general metal core found in complexes **1**–**3**. The same labelling scheme has been followed for all three complexes.

**Table 1.** Crystallographic parameters for complexes **1**–**3**.

| | **1** | **2** | **3** |
|---|---|---|---|
| formula | $C_{48}H_{68}N_4O_{25}Cl_2Dy_4$ | $C_{52}H_{72}N_4O_{25}Cl_2Tb_4$ | $C_{52}H_{72}N_4O_{25}Br_2Gd_4$ |
| size [mm] | 0.17×0.12×0.09 | 0.16×0.11x 0.08 | 0.16×0.13×0.09 |
| system | triclinic | triclinic | triclinic |
| space group | $P\bar{1}$ | $P\bar{1}$ | $P\bar{1}$ |
| *a* [Å] | 14.000(3) | 13.914(5) | 14.029(7) |
| *b* [Å] | 15.650(3) | 15.625(6) | 15.692(8) |
| *c* [Å] | 17.790(4) | 18.201(7) | 18.363(9) |
| $\alpha$[°] | 101.07(3) | 102.620(4) | 103.411(7) |
| $\beta$ [°] | 91.48(3) | 92.951(5) | 92.689(5) |
| $\gamma$[°] | 106.25(3) | 105.233(5) | 105.499(7) |
| *V* [Å$^3$] | 3659.3(13) | 3701(2) | 3764(3) |
| *Z* | 2 | 2 | 2 |
| $\rho_{calcd}$ [g cm$^{-3}$] | 1.654 | 1.669 | 1.714 |
| $2\theta_{max}$ | 47.64 | 58.26 | 50.64 |
| radiation | $Mo_{K\alpha}$ | $Mo_{K\alpha}$ | $Mo_{K\alpha}$ |
| $\lambda$ [Å] | 0.71073 | 0.71075 | 0.71073 |
| *T* [K] | 100 | 100 | 100 |
| reflns | 27407 | 65208 | 50807 |
| ind. reflns | 11213 | 19250 | 13500 |
| reflns with $I > 2\sigma(I)$ | 6798 | 15596 | 11560 |
| *R1* | 0.0660 | 0.0689 | 0.0806 |
| *wR2* | 0.1562 | 0.1825 | 0.2266 |

The lanthanide ions are in their usual trivalent oxidation state and occupy the corners of a square, at the center of which lies a $\mu_4\text{-}OH^-$ ion, linking all four lanthanide ions. The oxidation

state of this $\mu_4$-bridging O atom was confirmed by bond valence sum calculations (Table S1 in the Supporting Information).[18] The Ln ions are not coplanar; there is a small twist of 19° (for **1**) and 18.8° (for **2** and **3**) in the dihedral angle within the $Ln_4$ plane (Figure 2D). The $\mu_4$-$OH^-$ ion possesses a distorted

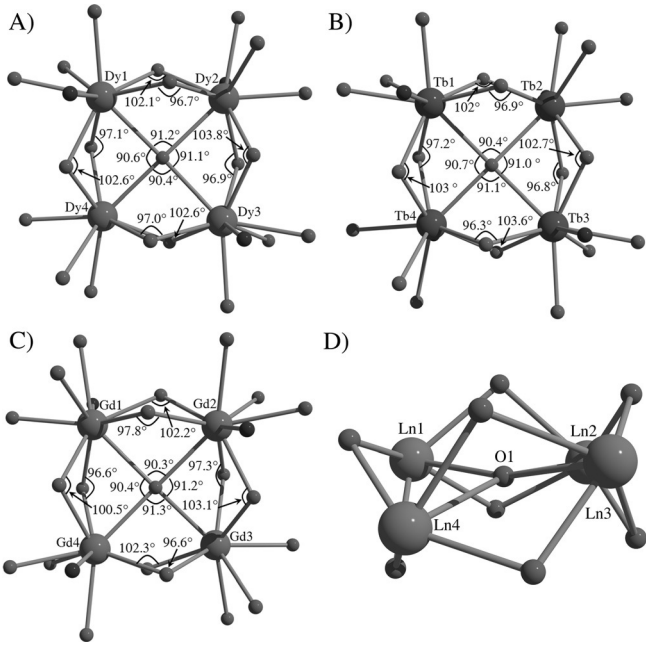


**Figure 2.** Average bond lengths and bond angles for **1**–**3** (A–C). D) A view to highlight the distortion in the $Ln_4$ square, with a Ln···Ln···Ln···Ln dihedral angle of 19°.

square planar geometry in all three complexes (Figure 2). The average diagonal bond angles found in these complexes are ∡Ln1O1Ln3 = 166.2° and ∡Ln2O1Ln4 = 166.6°.

The bond lengths between the $Ln^{III}$ ions and the central hydroxide ion range from 2.506 to 2.529 Å (for **1**), 2.494 to 2.553 Å (for **2**), and from 2.506 to 2.586 Å (for **3**). The average Ln–Ln distance is 3.577 (for **1**), 3.592 (for **2**), and 3.623 Å (for **3**). Each edge of the square is bridged by one phenoxo oxygen (from the *o*-vanillin moiety) from one $H_2L^{2-}$ and an alkoxo O atom from the hydroxymethyl arm of a second $H_2L^{2-}$ ligand. The remaining coordination sites of the Ln ions are filled by methoxy O atoms of *o*-vanillin, azomethine N atoms, the O atom from the second arm of the hydromethyl group of $H_2L^{2-}$ (the third arm of the latter remains protonated and nonbonded), and terminally bonded water and methanol molecules.

There is a significant difference in the observed Ln–O bond lengths between the bridging alkoxide (2.262–2.320(8) (**1**), 2.278–2.322(7) (**2**), and 2.297–2.362(8) Å (**3**)) and the terminally bonded alcohol (2.453–2.514(15) (**1**), 2.457–2.492 (10) (**2**), and 2.479–2.511(8) Å (**3**)), suggesting the latter to be protonated.

The charge-balance requirements further support the assumption of two halide counter ions present in the crystal lattice, balancing the 2+ cationic charge of the metal cluster. The nonbonded arm of the hydromethyl group of $H_2L^{2-}$ facilitates intermolecular hydrogen bonding (O13···O73 = 2.721(5); O33···O53 = 2.611(8); C12···O73 = 2.636(6); C17···O73 = 2.657(4) Å).

Careful analysis of the bond lengths of the noncoordinated hydromethyl groups of all the Schiff base ligands in **1** reveals that C19–O13 (1.332(17) Å) has a significantly shorter bond length than the other three (C39–O33 (1.401(18)), C59–O53 (1.425(20), C79–O73 (1.410(15) Å)). This suggests that only the C19–O13 arm is deprotonated. A similar trend is followed for complexes **2** and **3**. Each lanthanide ion in **1**–**3** is surrounded by nine donor atoms ($LnO_8N_1$) and exists in a distorted, monocapped, square, anti-prismatic geometry, as confirmed by continuous measurements with the SHAPE software.[19] The square [$Ln_4$-$\mu_4$-OH] core is rather rare, limited to only three complexes, based on a recent search (June 2015) of the Cambridge Structural Database (CSD).[20]

For example, Wong and co-workers reported the complex [$Ln_4(\mu_4\text{-}O)L_2(NO_3)_4(MeOH)_2$] (Ln = Gd and Tb; L = 1,3-bis(2-hydroxy-3-methoxybenzylamino)propan-2-ol) in 2001, in which the Ln ions are eleven coordinate,[20c] and Thompson et al. reported a series of [2x2] square grids of formula [$Ln_4(L1)_4(\mu_4\text{-}O)(\mu_2\text{-}1,1\text{-}N_3)_4$] (Ln = Dy and Tb) with carbohydrozone (L1) ligands.[20b,21] In the latter each metal ion is surrounded by nine donor atoms in a capped, square, anti-prismatic geometry.

## Magnetic susceptibility

Temperature-dependent direct current (dc) magnetic susceptibility measurements on polycrystalline samples of **1**–**3** were carried out between $T = 300$ and 2.0 K in an external magnetic field of $H = 0.1$ T (Figure 3). The observed room temperature $\chi_M T$ values of 55.60 (for **1**), 47.20 (for **2**), and 30.98 $cm^3 K mol^{-1}$ (for **3**) are slightly lower than the expected values of 56.67 ($g = 4/3$; $S = 5/2$; L = 5; $^6H_{15/2}$ for **1**), 47.25 ($g = 3/2$; $S = 3$; $L = 3$; $^7F_6$ for **2**), and 31.5 $cm^3 K mol^{-1}$ ($g = 2.0$; $S = 7/2$; $L = 0$, $^8S_{7/2}$ for **3**) for magnetically dilute $Dy^{III}$, $Tb^{III}$, and $Gd^{III}$ ions, respectively. The $\chi_M T$ values for **1** and **2** gradually decrease from room temperature to $T = 45$ K, likely due to the depopulation of $m_J$ levels, with the depopulation effects being more evident in **1** than in **2**. The $\chi_M T$ value drops rapidly below 45 K, and reaches a value of 25.4 (for **1**) and 26.99 $cm^3 K mol^{-1}$ (for **2**) at 5.0 and 2.5 K, respectively. On the contrary, for **3**, the $\chi_M T$ value remains constant from room temperature to $T = 100$ K, below which it steadily decreases to a value of 12.95 $cm^3 K mol^{-1}$ at 2.31 K. The decrease in $\chi_M T$ values for all three complexes at lower temperatures is due to the combined effects of some, or all, of the following phenomena: magnetic anisotropy (**1**, **2**), intramolecular antiferromagnetic exchange interactions, intermolecular dipolar exchange interactions, and thermal depopulation effects.

Isothermal magnetization $M(H)$ measurements performed on polycrystalline samples of **1**–**3** are summarized in Figure 3, with full details reported in the Supporting Information (Figures S2–S4). From Figure 3 it is evident that complexes **1** and **2** show saturation at approximately 19.3 and 15.3 $N\mu_B$ at 2.0 and 2.2 K, respectively. These values are approximately half the expected value for four noninteracting or very weakly coupled

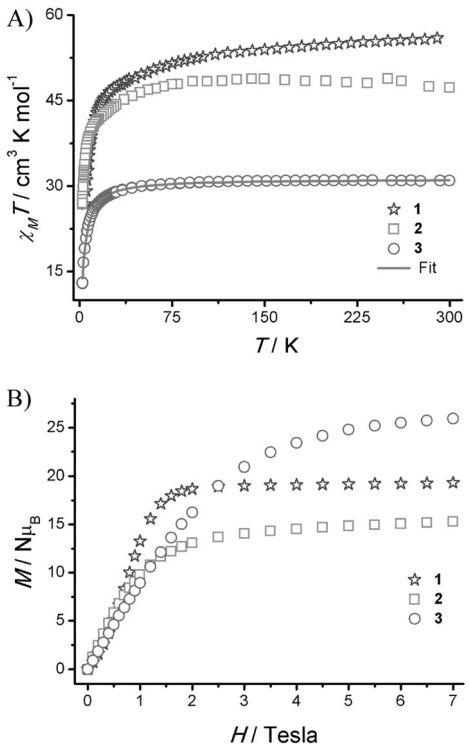


**Figure 3.** A) Variable-temperature $\chi_M T$ plots for complexes **1**–**3**, measured with an applied field of 0.1 T. The line denotes the best fit obtained for complex **3** with the parameters given in the text. B) Isothermal field-dependent magnetization measurements for **1**–**3** measured from $H=0$–7 T at $T=2.2$ K.

lanthanide ions, indicating the presence of significant magnetic anisotropy,[1h] and consistent with the non-superimposable reduced magnetization curves (Figure S5 in the Supporting Information). On the contrary, the magnetization of complex **3** is as expected for four weakly coupled, isotropic $Gd^{III}$ ions, with $M$ close to saturating at a value of 28 N$\mu_B$.

To extract the spin Hamiltonian parameters for the isotropic cluster **3**, magnetic susceptibility data were fitted by matrix diagonalization with the PHI software.[22] Based on the crystal structure parameters of **3**, we initially employed two different $J$ values: $J_1$ corresponds to nearest-neighbor interactions round the 'outside' of the square where the super-exchange interaction is mediated between the metal ions through phenoxo, alkoxo, and $\mu_4$-hydroxide bridges, and $J_2$ describes the next-nearest-neighbor (diagonal) interactions (Gd1O1Gd3 and Gd2O1Gd4) mediated exclusively by the central $\mu_4$-hydroxide. The Heisenberg Hamiltonian used for fitting the data is shown in the equation below. The experimental data are very well reproduced with the following parameters $J_1=-0.043$, $J_2=-0.043$ cm$^{-1}$ with $g=2.0$. Because $J_1=J_2$, we repeated the fit with just one $J$ value; which afforded $J_1=-0.043$ cm$^{-1}$ and $g=1.99$ (Figure 3). The fitting parameters clearly suggest that the exchange is very weak and the cluster can essentially be regarded as a paramagnet. Such weak exchange interactions between the metal centers are an essential ingredient for observing an enhanced MCE (see below).

$$H = -2(J_1 S_{Gd1} S_{Gd2} + J_1 S_{Gd2} S_{Gd3} + J_1 S_{Gd3} S_{Gd4} + J_1 S_{Gd1} S_{Gd4}) -2(J_2 S_{Gd1} S_{Gd3} + J_2 S_{Gd2} S_{Gd4}) + m_s g \mu_B H$$

To probe the magnetization relaxation dynamics of both **1** and **2**, ac magnetic susceptibility measurements were performed on polycrystalline samples of **1** (Figure 4) and **2** (Figure S6–S7 in the Supporting Information) at various frequencies. For **2**, the maxima in $\chi_M''$ is well below the instrument temperature limit in the presence and absence of an applied external dc magnetic field (Figure S7). On the contrary, for complex **1** there are two thermally assisted $\chi_M''$ signals with maxima clearly evident corresponding to fast and slow magnetization relaxation processes at low ($T=2.5$–5.2 K) and high ($T=3.0$–15 K) temperatures, respectively (Figure 4). Similar behavior was recently reported in related tetrameric clusters by Layfield and co-workers.[23] However, the origin of two magnetization relaxation processes in the latter complex are distinctly different from **1** (see below). Lanthanide complexes are prone

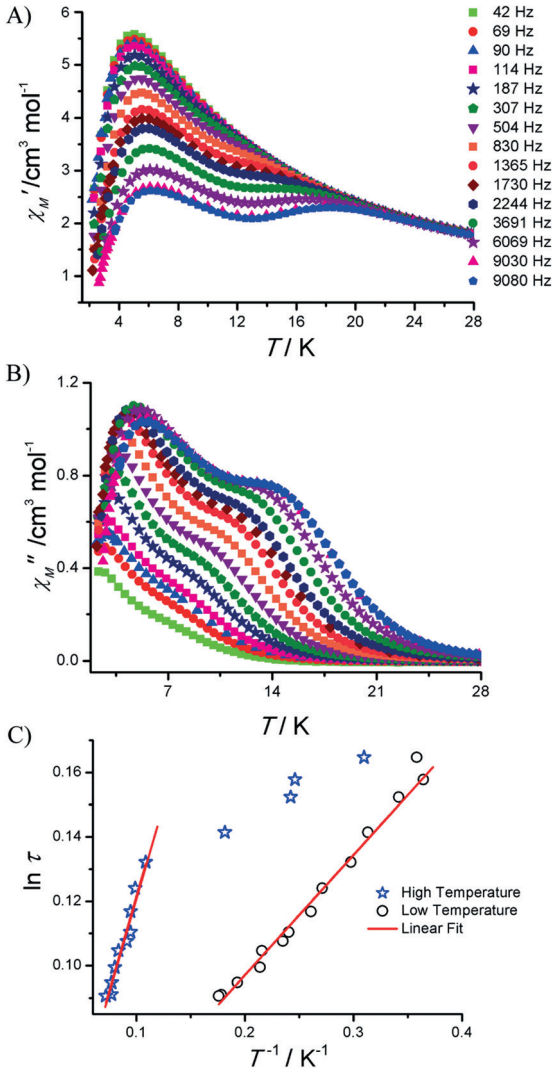


**Figure 4.** Frequency-dependent A) in-phase ($\chi_M'$) and B) out-of-phase ($\chi_M''$) ac magnetic susceptibility for **1** at the indicated frequencies. C) Arrhenius plot constructed for both slow and fast relaxation processes.

to exhibit fast quantum tunneling of magnetization (QTM),[1b] likely to be operable in the low-temperature region, however the thermally assisted Orbach process appears to be the dominant relaxation process in complex **1**. Observation of frequency dependent out-of-phase susceptibility ($\chi_M$") signals (for **1**) is a characteristic signature of SMM behavior under zero applied external magnetic field. The Arrhenius plot constructed for these high and low $T$ regimes are shown in Figure 4C. The $U_{eff}$ value for the reorientation of magnetization for the fast and slow relaxation processes are 29 and 100 K with $\tau_0 = 1.324 \times 10^{-7}$ and $1.179 \times 10^{-8}$ s, respectively. The deviation from linearity for the slow relaxation process below 7.0 K suggests that other relaxation processes, such as Raman and direct processes, are also likely to be operable.[10e,24]

The presence of two relaxations processes in ac data is clearly visible in the Cole–Cole plot (Figure 5). Attempts to fit the observed two relaxation processes with the generalized Debye

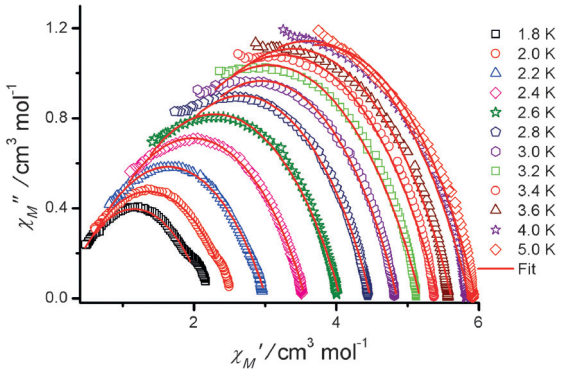


**Figure 5.** Cole–Cole plot of complex **1** measured in the absence of external magnetic field ($H_{dc} = 0$).

model failed; hence we fitted only the major relaxation process (Table S2 in the Supporting Information). The α-value ranges from 0.39 to 0.51. Further relaxation data have been measured for **1** in the presence of an external magnetic field of $H = 0.2$ T between $T = 2.0$–25 K. Figure S8 in the Supporting Information shows that the slow relaxation process observed at higher temperature is more prominent than the fast relaxation process observed at lower temperature.

The Arrhenius plot constructed for the high temperature relaxation process yields $U_{eff} = 194$ K with $\tau_0 = 6.38 \times 10^{-9}$ s. This experiment unambiguously confirms that QTM is one of the major relaxation processes in the ac relaxation dynamics in the absence of an external magnetic field. This could be the likely reason why the estimated energy barrier is significantly lower than the computed effective energy barrier (see below).[25]

To understand the electronic structures of anisotropic complex **1**, detailed ab initio calculations[26] were performed (see the Supporting Information for computational details and Figure S9). As complex **1** exhibits SMM characteristics, calculations were performed only on this structure. Two sets of calculations were performed on complex **1**. Primarily, using the SINGLE ANISO program,[27] we calculated the magnetic anisotropy of the individual $Dy^{III}$ ions. We then employed the POLY_ANISO program[28] to extract the exchange-coupled energy levels and the exchange parameters. We begin our discussion with the calculation of the single-ion anisotropy parameters, followed by a detailed analysis of the exchange spectrum.

### Single-ion anisotropy of $Dy^{III}$

The energy spectrum and $g$-tensors for the Kramers doublets (KDs) of the ground $^6H_{15/2}$ multiplet for the four $Dy^{III}$ ions in compound **1** are shown in the Supporting Information (Tables S3–S6), with the excited states lying at 3000 cm$^{-1}$. In **1**, the ground state (GS) KD (Figure 6) shows an almost Ising type anisotropy for all four metal sites (Table 2) that is, $g_{zz}$ is close to

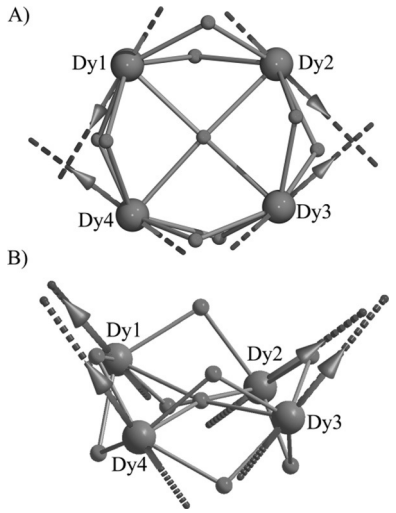


**Figure 6.** Ab initio computed ground KD state anisotropy axis along the $z$ direction in **1**. The arrows exhibit coupled-state orientations (ferromagnetic interaction between neighbors); N, C, and H atoms have been removed for clarity. The $g_{zz}$ orientations in all the $Dy^{III}$ sites differ due to the underlying structural distortions at the individual metal sites.

**Table 2.** Calculated energy spectrum, $g$ tensors and tilt angles ($\theta$) of the principal anisotropy axes of first excited state (ES) on Dy1, Dy2, Dy3, and Dy4 sites with respect to the GS for complex **1**.

| Sites | | $g_{xx}$ | $g_{yy}$ | $g_{zz}$ | Energy [cm$^{-1}$] | $\theta$ [°] |
|---|---|---|---|---|---|---|
| Dy1 | GS KD | 0.049 | 0.103 | 19.794 | 0.000 | – |
| | 1st ES KD | 0.976 | 1.982 | 15.819 | 134.6 | 14.6 |
| Dy2 | GS KD | 0.043 | 0.069 | 19.768 | 0.000 | – |
| | 1st ES KD | 1.192 | 3.127 | 14.998 | 147.8 | 10.5 |
| Dy3 | GS KD | 0.091 | 0.199 | 19.554 | 0.000 | – |
| | 1st ES KD | 1.799 | 5.654 | 12.629 | 145.0 | 5.5 |
| Dy4 | GS KD | 0.090 | 0.023 | 19.868 | 0.000 | – |
| | 1st ES KD | 0.168 | 0.253 | 16.968 | 190.0 | 168.9 |

20, with a small transverse anisotropy. The axiality of the $g$-tensors gradually decreases up to fourth KD (Tables S3–S6 in the Supporting Information), thereafter increasing and reaching axiality for the 8th KD, which is comparable to the value of lowest KD (close to 20). The observation of such mirror symmetry in the magnetic properties in the KDs is in sharp contrast to the trend in perfectly axial systems. The relative ener-

gies of the eight lowest lying KDs along with the computed anisotropy for all four $Dy^{III}$ ions in complex **1** are given in Tables S3–S6 in the Supporting Information. The ground state is found to possess zero magnetic moment in the *xy* plane and is entirely oriented along the z axis ($L_z$). The two lowest KDs, shown in Figure 6, are characterized by definite projection of the total angular moment of the anisotropy axis. At the Dy4 site the ground- and first-excited-state anisotropic axes are in opposite directions, whereas in the other three sites they are co-parallel.

To probe the mechanism of single-ion relaxation, data beyond the ground state KDs need to be analyzed. Magnetic relaxation of lanthanide species occurs due to three main factors in the absence of intermolecular interactions:[10e] 1) through QTM between the ground state KDs as a consequence of large transverse anisotropy in the ground state KDs, 2) through Orbach/Raman processes[29] which account for the relaxation via the excited states and occurs due to the non-coincidence of the principle anisotropic axes, and 3) through thermally assisted QTM (TA-QTM), which accounts for relaxation via the excited states due to the non-Ising nature of the excited KDs. A qualitative mechanism of the relaxation for **1** obtained from ab initio calculations is shown in Figure 7. Here the states are arranged according to the values of the magnetic moments. The number at each arrow connecting any two states is the mean absolute value of the matrix elements of the transition magnetic moments between the corresponding states. For all the Dy sites (Dy1, Dy2, Dy3, and Dy4) the transverse anisotropy observed is small, and QTM between the ground state KDs is expected to be weak.

Our calculations confirm this point, as shown in Figure 7; for both the Dy1 and the Dy4 center the QTM between the ground state KDs is negligible. The next excited states are located at 135, 148, and 145 $cm^{-1}$ for the Dy1, Dy2, and Dy3 centers, respectively, and these states possess significant transverse anisotropy. The $g_{zz}$ axis deviates from the direction of the ground state KD by 14.6, 10.47, and 5.47° for the Dy1, Dy2, and Dy3 centers, respectively (tilt angle, $\theta$). This naturally activates the Orbach/Raman type relaxation via the first excited state and, as expected, a significant magnetic moment matrix element is observed for this process (Figure 7 A). The transverse anisotropy of the first excited state is large; this leads to a significant TA-QTM process, which is also reflected in the computed parameters. The ground and first excited state are predominantly $|\pm 15/2>$: 0.99$|\pm 15/2>$ and $|\pm 3/2>$: 0.91$|\pm 13/2>$, respectively, for the Dy1, Dy2, and Dy3 sites.

The Dy4 site on the other hand is distinctly different from the other three sites in complex **1**, where the transverse anisotropy is not prominent in the ground state or the first excited state. However, the tilt angle is large, which leads to relaxation via the first excited state. Thus for Dy4, the computed effective energy barrier ($U_{cal}$) is 190.0 $cm^{-1}$, which is marginally higher than for the other sites. Thus, for the uncoupled $Dy^{III}$ sites, two relaxation processes are theoretically expected to operate, one at an average $U_{cal}$ of 144 $cm^{-1}$ (Dy1, Dy2 and Dy3) and the other at 190 $cm^{-1}$ (Dy4).

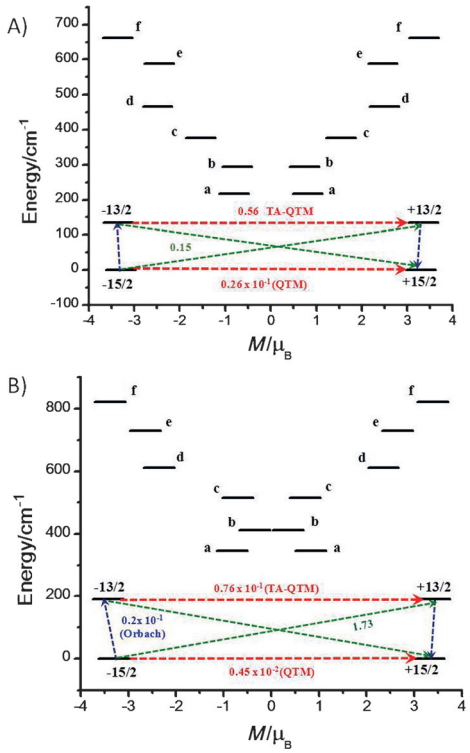


**Figure 7.** The ab initio computed magnetization blocking barriers for A) the Dy1 site (similar energy levels are found for the Dy2 and Dy3 sites) and B) the Dy4 site. The black lines indicate the KDs as a function of magnetic moment. The dotted green lines show the possible Orbach processes. The dotted blue lines show the most probable relaxation pathways for magnetization reversal. The dotted red lines represent the presence of QTM/TA-QTM between connecting pairs. All excited states for the Dy1/Dy2/Dy3 and Dy4 sites in complex **1** are strong admixtures of different $\pm m_J$ levels. Hence, the mixing of these wavefunctions has been represented by letters for which the corresponding wavefunction descriptions have been described in the computational section of the Supporting Information.

In accordance with the theoretical prediction, there are two relaxation processes that are experimentally observed at 20.15 and 69.5 $cm^{-1}$ (29 and 100 K respectively, Figure 4). Hence, we can tentatively assign the faster relaxation process, which occurs at lower temperature, to the Dy1, Dy2, and Dy3 sites, and the slower magnetization relaxation process, which occurs at higher temperature, to Dy4. The large deviation in the $U_{eff}$ values between the calculated and experimental results can be attributed to the fact that the ground state QTM and the dipolar/exchange interactions (intra and inter) are not taken into account in the estimate of the computed barriers. Attempts to isolate the diamagnetic analogue (using $Y^{III}$, $La^{III}$, or $Lu^{III}$) of complexes **1**–**3** were not successful. However, we would like to emphasize that the above-listed parameters significantly influence the experimental barrier height as shown by us in an unrelated $Er^{III}$ complex, for which a tenfold increase in $U_{eff}$ was observed with and without dilution (50 and 5 K).[30] We believe a similar scenario is also operational for complex **1**. The argument of magnetization relaxation based on single-ion anisotropy is valid because the estimate of the exchange coupling between the $Dy^{III}$ ions is extremely small (see below).

To offer a rationale on the differences observed between the four Dy sites, we have examined the structural distortion (using the SHAPE software)[19] at the individual Dy sites. The deviations are found to be 1.18, 1.22, 1.20, and 1.08 for the Dy1, Dy2, Dy3, and Dy4 sites, respectively (see Figure S9 in the Supporting Information), compared with an ideal, monocapped, square anti-prismatic geometry.

Thus the larger distortion of Dy1, Dy2, and Dy3 compared with Dy4 leads to concomitant smaller barrier heights. To gain more insight into the mechanism of magnetization relaxation, we have also computed the crystal-field parameters. If the intermolecular and hyperfine interactions are small or negligible, the probability of a QTM between the ground state KDs is best described by the crystal-field (CF) parameters.[10h,31] The corresponding CF Hamiltonian can be expressed as, $H_{CF}=B_k^q O_k^q$, where $B_k^q$ represents the crystal field parameter and $O_k^q$ represents the Stevens operator. Preponderantly larger (see Table S18 in the Supporting Information) nonaxial $B_k^q$ (where $q \neq 0$ K $=2,4,6$) terms compared with the corresponding axial $B_k^q$ (where $q=0$ K $=2,4,6$) terms are found to favor the QTM process (Table S7 in the Supporting Information).

The observation of a small transverse anisotropy for all the Dy sites in **1** is also well reproduced in the computed CF parameters, where the nonaxial terms are larger than the axial terms (Table S7 in the Supporting Information). We also employed an electrostatic model to gain information on the orientation of the anisotropy axis of the GS in complex **1**.[32] This axis is calculated to be close to the GS ab initio anisotropic axis, with a deviation of approximately 12.91, 9.28, 14.09, and 12.45° for Dy1, Dy2, Dy3, and Dy4, respectively (Figure S9 in the Supporting Information); this suggests that the orientation of the anisotropy axis is controlled predominantly by the electrostatic charges of the ligands.

### Exchange-coupled molecule

Due to the axiality of the Dy sites, we simulated the magnetic interactions between the Dy ions by incorporating contributions from magnetic dipole–dipole and exchange interactions within an Ising exchange Hamiltonian. We also calculated the exchange spectrum (Figure 8) of complex **1** by using the POLY_ANISO program. An excellent agreement between the simulated and experimental magnetic data ($\chi_M T$ ($T$) and $M$ ($H$)) was observed with the parameters $J_1 = +0.01$ cm$^{-1}$ and $J_2 = -0.01$ cm$^{-1}$ (Figure 9). This is further corroborated by specific heat measurements that show a well-defined Schottky anomaly at liquid-helium temperatures (see below). Our computed $g$-tensor for the exchange-coupled system shows zero transverse anisotropy contribution in the GS.

Most importantly, the principal $g$-tensor (magnetic moment, Table S8 in the Supporting Information) anisotropy of the lowest (ground) exchange level of the exchange spectrum is 3.96. The observation of a conventional magnetic moment (a deviation from zero) in the GS can be ascribed to the low-symmetry nature of the complex. The first excited doublet of the exchange spectrum lies at a larger energy separation (4.4 cm$^{-1}$) with respect to the GS, compared with a previously

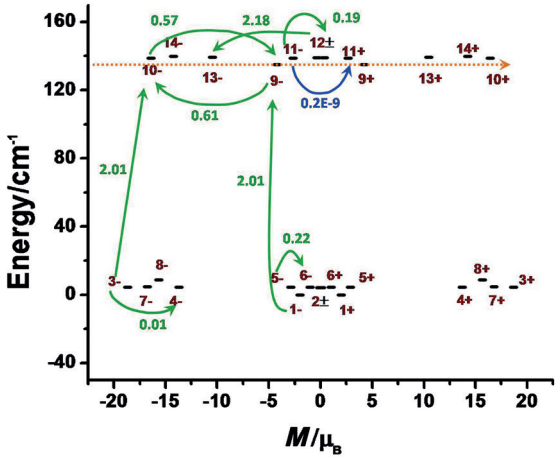


**Figure 8.** The low-lying exchange spectrum and magnetization blocking barrier in complex **1.** We have placed all exchange states in compliance with the value of the magnetic moments (bold black lines).The blue curved arrows signify tunneling of magnetization within each doublet state, green curved arrows represent spin-phonon transitions (the numbers are averaged transition moments in $\mu_B$ connecting the corresponding states).[34] For the transition moment matrix elements, only values below $0.2\times10^{-9}$ $\mu_B$ are shown (blue arrow); these correspond to the tunnelling between the states.

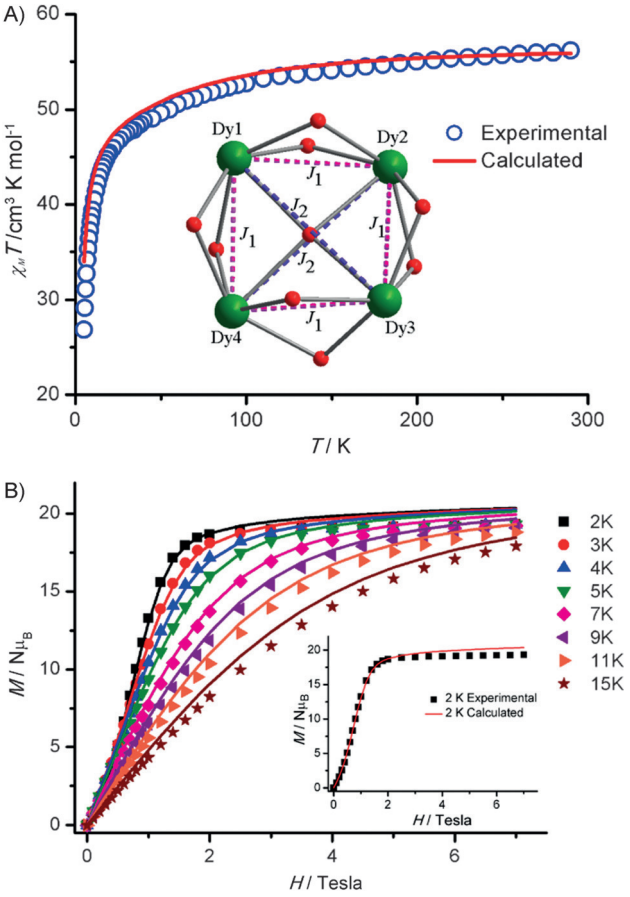


**Figure 9.** Poly_ANISO simulated (solid lines) A) magnetic susceptibility and B) magnetization data with respect to experimental data in complex **1**. The intermolecular interaction ($zJ'$) was fixed at $-0.14$ cm$^{-1}$.

studied $Dy_4$ complex[33] (2.97 $cm^{-1}$), which introduces a very small low field S shape to the magnetization curve (Figure 9B inset) in complex **1.**

This intramolecular coupling may facilitate preferential information storage compared with conventional SMMs.[7b] An analysis of the exchange spectrum of **1** (Table S8 in the Supporting Information) clearly reveals a small magnetic-moment matrix element for the GS exchange doublet (non-Kramers system), which subsequently suppresses the QTM completely (Figure 8, Table S8).

The values for all other low-lying states (including excited states) are found to have low magnitudes, resulting in complete suppression of TA-QTM contributions to the magnetic relaxation. These observations lead to the occurrence of relaxation via a spin-phonon tunnelling mechanism through the excited states, as indicated by the green arrows in Figure 7.

Significant matrix elements computed between $\pm5$ and $\pm6$ describes a barrier for magnetization reversal of approximately 4.6 $cm^{-1}$ (Figure 8, Table S8 in the Supporting Information). Another important spin-phonon transition has been observed from the GS $-1$ component to the $-9$ excited state components, followed by transition from $-9$ to $-10$, $-10$ to $-11$, $-11$ to $-12$, $-12$ to $-13$, and eventually to the time-reversed states in the opposite order (green arrows in Figure 8).

This is the sole pathway with substantial magnetic matrix elements connecting GS $-1$ with other excited states. Additionally, direct tunnelling transitions between higher excited states (i.e., between $-9$ and $+9$, $-10$ and $+10$) are less efficient due to the extremely small value of magnetic-moment matrix elements that are of the order of $10^{-10}$ $\mu_B$. Hence, another barrier height can be envisioned to occur at approximately 138 $cm^{-1}$ (as shown by the dotted orange line in Figure 8), which is similar to the slower magnetization relaxation observed from the ac susceptibility measurements. The observation of such a multilevel-exchange spectrum corroborates the presence of a slow magnetization relaxation time in complex **1** due to the significantly quenched QTM and TA-QTM processes. As the exchange interactions are extremely small, at lower temperatures, the individual Dy sites are expected to have independent orientation and the small exchange coupling results in a fluctuating magnetic field leading to a very fast relaxation.[35]

The calculated ab initio and electrostatic anisotropy axes lie at a position that faces the least repulsion from the negatively charged $\mu_4$-hydroxo ligand. Although not all four $g_{zz}$ axes create a circular pattern, the projected magnetic moment due to $g_{zz}$, which is in the plane of the four lanthanide ions, leads to a toroidal magnetic moment.[7b,36] This is rather clearly visible in the magnetization data measured at $T=2$ K, and similar to the toroidal moments observed in other Dy structures, such as the $Dy_6$ wheel, $Dy_3$ triangles, and $Dy_4$ butterfly complexes.[8,33,36–37] Analysis of the structural details of complex **1** indicates that it possesses a *pseudo* $C_4$ axis of symmetry.

The $g_{zz}$ axis of Dy1, Dy2, and Dy3 are in plane with respect to the pseudo $C_4$ axis, with tilts of 6.2°, 15.9°, and 13.2° for Dy1, Dy2 and Dy3, respectively (Figure 6) and the deviations are within approximately 10°. The Dy4 ion on the other hand deviates significantly from the pseudo $C_4$ axis with a tilt angle of 41.5°. However, the projected magnetic moment of all four Dy sites is expected to be on the square plane of the molecule leading to a toroidal moment. Although analogous square-based complexes have been reported in the literature,[20b,c,21] this is the first example to show toroidal magnetic moment in this family; this is strongly corroborated by ab initio calculations.

### Estimation of magnetocaloric effect (MCE)

To evaluate the MCE efficiency of all three complexes (**1**–**3**), detailed magnetization measurements (see the Supporting Information, Figures S2–S4) and field-dependent heat-capacity (Figure 10) measurements were performed on bulk samples. Change in magnetic entropy ($-\Delta S$) and temperature ($\Delta T_{ad}$) of the molecular cluster are the two essential thermodynamic parameters of MCE; these can be extracted from magnetization measurements by using Maxwell's thermodynamic relation:

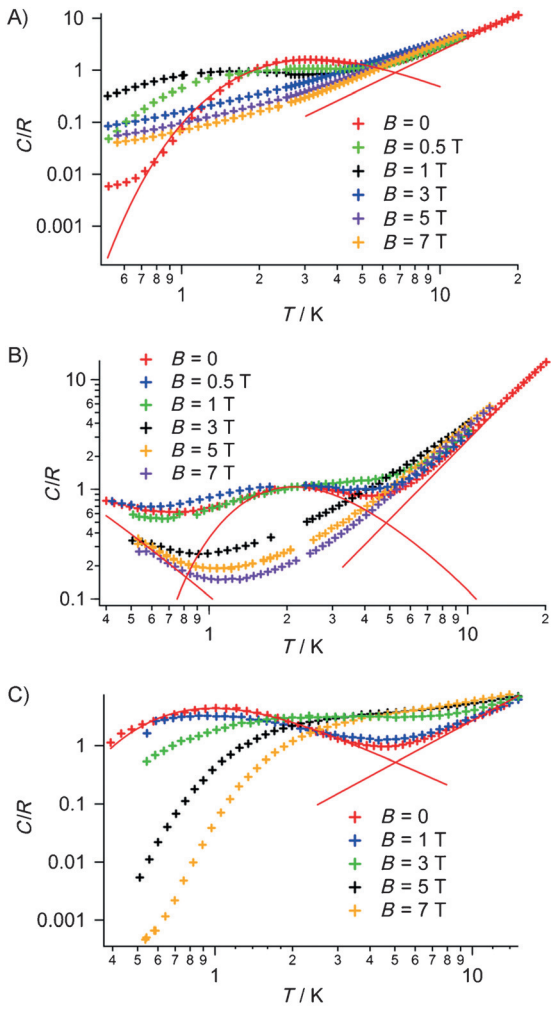


**Figure 10.** A–C) Temperature dependence of the heat capacity measured on polycrystalline samples of **1**–**3** at the indicated magnetic field (data normalized to the gas constant *R*). Markers indicate the experimental data and lines are the calculations described in the text.

$$\Delta S_m(T,H) = \int_{H_i}^{H_f} [\frac{\partial M(T,H)}{\partial T}]_H dH$$

where $H_i$ and $H_f$ are the initial and final applied magnetic field, respectively.

To validate the $-\Delta S_m$ value extracted from magnetization measurements for **1**–**3**, heat-capacity measurements were also performed on polycrystalline samples at various applied magnetic fields (Figure 10). A large field-independent contribution is observed above approximately 5 K; this is attributed to the lattice. This lattice contribution can be modelled by using an effective Debye model[38] $C_{latt} = A\,T^{\alpha}$, with $\alpha = 2.4$ (for **1**, **2** and **3**) and phenomenological coefficient ($A$), which was found to be $0.0095 \pm 10\%$ (for **1**), $A = 0.011 \pm 10\%$ (for **2**), $A = 0.010 \pm 10\%$ (for **3**). This contribution is comparable for the three molecules, as expected from the nearly identical structures.

A Schottky anomaly is evident in the low-temperature specific heat of all three derivatives with a maximum at 1–2 K, arising from the magnetic-exchange interactions between the magnetic ions. To get a rough idea of the strength of the interaction, we modelled this Schottky anomaly by considering an effective split between two equally degenerate states separated by an energy gap $T_0$.

$$C_{int}/R = B\,(T_0/T)^2\,e^{(T_0/T)}/(1+e^{(T_0/T)})^2$$

Data fitting on the three $C(T)$ curves provides these values for the parameters $B = 3.7$ T and $T_0 = 7.78$ K for **1**, $B = 2.45$ T and $T_0 = 5.1$ K for **2**, $B = 10$ T and $T_0 = 2.35$ K for **3**. In a first approximation the mean value of the exchange interactions $J_{SE}$ between four lanthanides leads to an effective gap $T_0 = 6J^2\,g_J^2\,J_{SE}$.

In this way we are considering six equivalent interactions between the four magnetic ions, so what is found here is a mean value for $J_{SE}$. We found for **1** $J_{SE} = 0.0131$ K, for **2** $J_{SE} = 0.0105$ K and for **3** $J_{SE} = 0.0080$ K, comparable to $J_1$ and $J_2$ values theoretically estimated above. For **2**, another term is required to describe the upturn of the specific heat below 0.7 K: the hyperfine coupling can be modelled by using the hyperfine energy levels of terbium (0.120, 0.149, and 0.178 K) as respective gaps between the four hyperfine sublevels of the $J = 6$ multiplet and a multilevel Schottky anomaly expression.

The magnetic entropy ($S_m$) can also be evaluated from $S_m(T,H) = \int C_m/TdT$ where $C_m$ is magnetic heat capacity directly obtained from heat-capacity measurements. Notably, the extracted values are consistent with the values obtained from magnetization measurements. As expected, complex **3**, shows the largest $-\Delta S_m$ among the three complexes (Figure 11). The maximum value obtained for a 7 T–0 demagnetization is $-\Delta S_m = (5.8 \pm 0.6)\,R = 23$ J Kg$^{-1}$ K$^{-1}$ at $T \approx 3$ K for **3**; $-\Delta S_m = (2.2 \pm 0.4)\,R$ at $T \approx 6$ K for **1** and $-\Delta S_m = (2.0 \pm 0.4)\,R$ at $T \approx 5$ K for **2** (Figures S10–S11 in the Supporting Information).

The zero-field splitting due to large spin–orbit coupling associated with **1** and **2** results in significantly lower degeneracy of the GS. This leads to a smaller change in the magnetic-entropy value compared with more isotropic clusters. Such scenarios have been witnessed already in other lanthanide–metal complexes.[14h, 39]

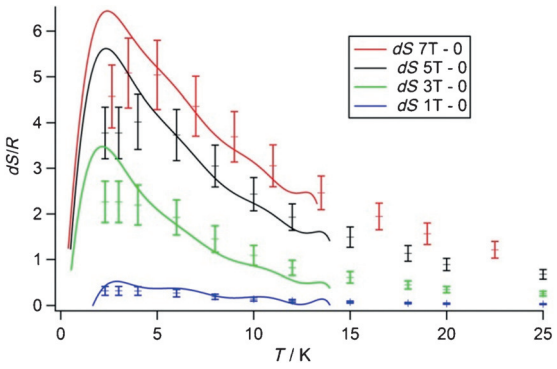


**Figure 11.** Entropy variation estimated from both magnetization measurements (points) and specific heat measurements (lines) for **1** for different magnetic field changes.

The observed $-\Delta S_m$ value for **3** is one of the largest known for an isotropic complex, however this is significantly lower than for the other isotropic metal complexes reported in the literature.[14e, h, 16, 40] Interestingly, the $-\Delta S_m$ value expressed in J kg$^{-1}$ K$^{-1}$ for **3** is larger than that reported for $Gd_4Zn_8$,[14c] which contain a similar square $Gd_4$ core; this is in part due to the lighter mass of our **3** derivative, confirming the strategy of using a lighter compound to enhance the MCE.

For four uncoupled $Gd^{III}$ ions, the theoretically expected $-\Delta S_m$ value is 20.8 J kg$^{-1}$ K$^{-1}$, however, experimentally we observe a value that is higher than the uncoupled one; signifying that the excited states also participate in polarizing the spins. Accessibility of possible excited states in the case of **3**, even at low temperatures, is likely due to the weak exchange interactions.

## Conclusion

We have reported an unusual family of O-centered $Ln_4$ (where Ln = Dy, Tb or Gd) squares, the structures of which were determined by single-crystal X-ray diffraction. Dc magnetic susceptibility data on complexes **1**–**3** show weak antiferromagnetic interactions between the metal ions. Unambiguous evidence for the existence of antiferromagnetic interactions between the anisotropic lanthanide ions is confirmed through ab initio calculations and heat-capacity measurements. Measurements of the ac susceptibility of the anisotropic complexes **1** and **2** in the 2–35 K temperature range reveal both complexes to show frequency-dependent out-of-phase signals ($\chi_M$"), although the maxima in $\chi_M$" for **2** is below the temperature limit of our instrument. On the other hand, complex **1** shows two different magnetization relaxation processes, one at high temperature and one at low temperature. The Arrhenius plot constructed from these two relaxation processes gives energy barriers for the reversal of the magnetization vector at 29 and 100 K. We have rationalized the origin of these two relaxations processes in complex **1** by detailed ab initio calculations, which demonstrated that the Dy4 site in complex **1** behaves differently compared with the other three sites. Calculations reveal the existence of a toroidal magnetic moment in complex **1**; confirmed experimentally by the S-shaped magnetization curve at 2.0 K.

The exchange interaction extracted from the POLY_ANISO program is in agreement with experimentally derived parameters. The MCE of all the three complexes were estimated from two different experimental techniques, field-dependent magnetization and heat-capacity measurements. Complex **3** shows the largest change in magnetic entropy (23 $J\,Kg^{-1}\,K^{-1}$), due to the near isotropic nature of the GS and weak exchange interactions. The three, analogous, square-based complexes are therefore a family of complexes exhibiting a variety of physical properties, including toroidal magnetic moments, SMM behavior, and enhanced MCE.

## Experimental Section

All reagents and solvents were purchased from commercially available sources (Alfa Aesar and Sigma-Aldrich) and were used without further purification. All reactions were carried out under aerobic conditions unless otherwise stated. The ligand $H_4L$ was synthesized as per the literature report,[17o] with a slight modification to improve the yield of the reaction; see below for details. The chosen crystal was mounted on a Goniometer with the use of paraffin oil and the crystal cooled in a stream of liquid nitrogen to 100 K (for **1** and **3**). For **2**, data were collected at room temperature. The data collection was done on a Rigaku Saturn CCD diffractometer (for **1** and **3**) and an Oxford CCD diffractometer for **2** with a graphite monochromator ($\lambda = 0.71073^{\circ}$) equipped with an Oxford cryosystems cooler device. The unit cell determination and data reduction were performed with the Rigaku CrystalClear-SM Expert 2.1 software. The structures were solved by direct methods and the refined by least-squares procedures on $F^2$ with SHELXTL package. All non-hydrogen atoms were refined anisotropically. Hydrogen atoms were placed based on the geometry and refined with a riding model. The solvent molecules were heavily disordered and could not be model due to diffused electron density in all three complexes. The SQUZEE routine from PLATON resulted in smooth refinement of the structures. The loop corresponding to residual electron-density voids (from PLATON) is appended in the corresponding CIF files.

NMR spectra for the $H_4L$ ligand were recorded on a Bruker Avance III 400 MHz instrument at room temperature. The data were calibrated with listed deuterated solvents. Infrared spectra were collected for the solid samples by using KBr pellets on a PerkinElmer FT-IR spectrometer in the 400 to 4000 $cm^{-1}$ range. Variable-temperature dc susceptibility measurements were performed on a quantum design MPMS-SQUID magnetometer. Diamagnetic corrections were applied for the constituent atoms by using Pascal's constants. Heat-capacity measurements were measured on a PPMS-7T system by using the two-tau method. Microcrystals were pressed into thin pellets and cut in thin slices of 1–2 mg in weight.

### Synthesis of $H_4L$

In a 250 mL round-bottom flask a methanolic solution of *o*-vanillin (5.0002 g, 0.0328 mol, 100 mL MeOH) was added glacial acetic acid (0.3 mL, 5–6 drops) dropwise to activate the carbonyl group in *o*-vanillin and stirred for 10 min. Into the reaction flask, solid tris(hydroxymethyl)aminomethane (3.981 g, 0.0328 mol) was then added and the reaction mixture was heated to reflux for 24 h. The light-yellow precipitate that formed was filtered and washed with *n*-hexane several times and dried under vacuum. Yield = 7.56 g, 90%. The purity of the ligand was confirmed by $^1H$ and $^{13}C$ NMR recorded in [$D_6$]DMSO. $^1H$ NMR (400 MHz): $\delta = 14.7$(s, 1H), 8.48(s, 1H), 6.92 (dd, $J = 7.88$ Hz, 2H), 6.57 (t, $J = 7.84$ Hz, 1H), 4.84 (s, 3H), 3.73 (s, 3H), 3.6 ppm (d, 6H); $^{13}C$ NMR $\delta = 164.11$(C=N), 158.17, 149.53, 124.15, 117.12, 114.86, 114.33, 66.43, 61.11, 55.72 ppm; FT-IR (KBr pellet): $\tilde{\nu} = 2919$ (s, $\nu$(Ar−H)), 1644 $cm^{-1}$ (s, $\nu$(C=N)).

### Synthesis of complex 1

A methanolic solution (30 mL) of $H_4L$ (0.300 g, 1.175 mmol) was deprotonated by using NaOMe (0.1269 g, 2.350 mmol) and the solution stirred for 30 min before charging $DyCl_3{\cdot}6H_2O$ (0.3159 g, 1.175 mmol) into the reaction flask. The resultant reaction mixture was stirred for 24 h and then filtered. The filtrate volume was reduced to one third of the initial volume and kept for crystallization without any disturbance. Pale, yellow, block-shaped, single crystals grew from the filtrate after one week, and were suitable for X-ray diffraction. Yield: 142 mg (27%, based on Dy). Elemental analysis (air dried sample) calcd (%): C 29.8, H 4.9, N 2.7; found: C 30.1, H 4.6, N 2.6; FT-IR (KBr pellet): $\tilde{\nu} = 2921$ (s, $\nu$(Ar−H)), 1648 $cm^{-1}$ (s, $\nu$(C=N)).

### Synthesis of complexes 2 and 3

The same procedure was followed for complex **1**, by using the corresponding equivalence of lanthanide halides ($TbCl_3{\cdot}6H_2O$ (0.4388 g, 1.175 mmol for **2** and $GdBr_3{\cdot}6H_2O$ (0.4665 g, 1.175 mmol) for **3**) in place of $DyCl_3.6H_2O$. For **2**: yield: 137 mg (25%, based on the Tb). Elemental analysis (air dried sample) calcd (%): C 32.6, H 4.7, N 2.7; found: C 32.1, H 4.8, N 2.6; FT-IR (KBr pellet): $\tilde{\nu} = 2924$ (s, $\nu$(Ar−H)), 1644 $cm^{-1}$ (s, $\nu$(C=N)). For **3**: yield: 145 mg (26%, based on the Gd). Elemental analysis (dried sample) calcd (%): C 31.6, H 4.6, N 2.6; found: C 31.2, H 4.7, N 2.6; FT-IR (KBr pellet): $\tilde{\nu} = 2926$ (s, $\nu$(Ar−H)), 1646 $cm^{-1}$ (s, $\nu$(C=N)).

Crystal structures of all the three complexes and magnetic data (both dc and ac data) are given in the Supporting Information, along with full computational details. CCDC 1060622 (**1**), 1060623 (**2**), and 1060624 (**3**) contain the supplementary crystallographic data for this paper. These data are provided free of charge by The Cambridge Crystallographic Data Centre.

## *Acknowledgements*

MS likes to thank CSIR (01(2768)/13/EMR-II), DST (SR/S1/IC-32/2011), DST-Nanomission (SR/NM/NS-1119/2011), and IIT Bombay for financial support. GR thanks DST-Nanomission (SR/NM/NS-1119/2011), AISRF. EKB thanks the EPSRC. MS and GR thank Dr. Ungur and Prof. Chibotaru, Belgium, for their additional MOLCAS routine and we are indebted to Dr. Ungur for providing us the POLY_ANISO code for our computational study.

**Keywords:** ab initio calculations · clusters · dysprosium · magnetism · magnetocaloric effect

[1] a) G. Aromí, E. K. Brechin, *Struct. Bonding (Berlin)* **2006**, *122*, 1–67; b) R. J. Blagg, L. Ungur, F. Tuna, J. Speak, P. Comar, D. Collison, W. Wernsdorfer, E. J. L. McInnes, L. F. Chibotaru, R. E. P. Winpenny, *Nat. Chem.* **2013**, *5*, 673–678; c) D. Gatteschi, A. Caneschi, L. Pardi, R. Sessoli, *Science* **1994**, *265*, 1054–1058; d) M. Mannini, F. Pineider, C. Danieli, F. Totti, L. Sorace, P. Sainctavit, M. A. Arrio, E. Otero, L. Joly, J. C. Cezar, A. Cornia, R. Sessoli, *Nature* **2010**, *468*, 417–421; e) M. Mannini, F. Pineider, P. Sainctavit, C. Danieli, E. Otero, C. Sciancalepore, A. M. Talarico, M.-A. Arrio, A. Cornia, D. Gatteschi, R. Sessoli, *Nat. Mater.* **2009**, *8*, 194–197;

 

f) R. Sessoli, D. Gatteschi, A. Caneschi, M. A. Novak, *Nature* **1993**, *365*, 141 – 143; g) R. Sessoli, H. L. Tsai, A. R. Schake, S. Wang, J. B. Vincent, K. Folting, D. Gatteschi, G. Christou, D. N. Hendrickson, *J. Am. Chem. Soc.* **1993**, *115*, 1804 – 1816; h) D. N. Woodruff, R. E. P. Winpenny, R. A. Layfield, *Chem. Rev.* **2013**, *113*, 5110 – 5148.

[2] a) L. Bogani, W. Wernsdorfer, *Nat. Mater.* **2008**, *7*, 179 – 186; b) S. Sanvito, A. R. Rocha, *J. Comput. Theor. Nanosci.* **2006**, *3*, 624 – 642; c) W. Wernsdorfer, *Int. J. Nanotechnol.* **2010**, *7*, 497 – 522.

[3] a) C. P. Collier, G. Matterstei, E. W. Wong, Y. Luo, K. Beverly, J. Sampaio, F. M. Raymo, J. F. Stoddart, J. R. Heath, *Science* **2000**, *289*, 1172 – 1175; b) A. R. Pease, J. O. Jeppesen, J. F. Stoddart, Y. Luo, C. P. Collier, J. R. Heath, *Acc. Chem. Res.* **2001**, *34*, 433 – 444.

[4] a) F. R. Renani, G. Kirczenow, *Phys. Rev. B* **2013**, *87*, 121403; b) M. Urdampilleta, S. Klyatskaya, J. P. Cleuziou, M. Ruben, W. Wernsdorfer, *Nat. Mater.* **2011**, *10*, 502 – 506.

[5] D. Aguilà, L. A. Barrios, V. Velasco, O. Roubeau, A. Repolles, P. J. Alonso, J. Sese, S. J. Teat, F. Luis, G. Aromi, *J. Am. Chem. Soc.* **2014**, *136*, 14215 – 14222.

[6] N. Ishikawa, M. Sugita, T. Ishikawa, S.-Y. Koshihara, Y. Kaizu, *J. Am. Chem. Soc.* **2003**, *125*, 8694 – 8695.

[7] a) H. L. C. Feltham, S. Brooker, *Coord. Chem. Rev.* **2014**, *276*, 1 – 33; b) L. Ungur, S.-Y. Lin, J. Tang, L. F. Chibotaru, *Chem. Soc. Rev.* **2014**, *43*, 6894 – 6905; c) R. A. Layfield, *Organometallics* **2014**, *33*, 1084 – 1099; d) L.-X. Chang, G. Xiong, L. Wang, P. Cheng, B. Zhao, *Chem. Commun.* **2013**, *49*, 1055 – 1057.

[8] J. Tang, I. Hewitt, N. T. Madhu, G. Chastanet, W. Wernsdorfer, C. E. Anson, C. Benelli, R. Sessoli, A. K. Powell, *Angew. Chem. Int. Ed.* **2006**, *45*, 1729 – 1733; *Angew. Chem.* **2006**, *118*, 1761 – 1765.

[9] J. D. Rinehart, M. Fang, W. J. Evans, J. R. Long, *J. Am. Chem. Soc.* **2011**, *133*, 14236 – 14239.

[10] a) M. A. AlDamen, S. Cardona-Serra, J. M. Clemente-Juan, E. Coronado, A. Gaita-Arino, C. Marti-Gastaldo, F. Luis, O. Montero, *Inorg. Chem.* **2009**, *48*, 3467 – 3479; b) M. A. AlDamen, J. M. Clemente-Juan, E. Coronado, C. Marti-Gastaldo, A. Gaita-Arino, *J. Am. Chem. Soc.* **2008**, *130*, 8874 – 8875; c) S. Cardona-Serra, J. M. Clemente-Juan, E. Coronado, A. Gaita-Arino, A. Camon, M. Evangelisti, F. Luis, M. J. Martinez-Perez, J. Sese, *J. Am. Chem. Soc.* **2012**, *134*, 14982 – 14990; d) S. Ghosh, S. Datta, L. Friend, S. Cardona-Serra, A. Gaita-Arino, E. Coronado, S. Hill, *Dalton Trans.* **2012**, *41*, 13697 – 13704; e) N. Ishikawa, M. Sugita, T. Ishikawa, S. Koshihara, Y. Kaizu, *J. Phys. Chem. B* **2004**, *108*, 11265 – 11271; f) N. Ishikawa, M. Sugita, N. Tanaka, T. Ishikawa, S.-Y. Koshihara, Y. Kaizu, *Inorg. Chem.* **2004**, *43*, 5498 – 5500; g) J. Kan, H. Wang, W. Sun, W. Cao, J. Tao, J. Jiang, *Inorg. Chem.* **2013**, *52*, 8505 – 8510; h) J. J. Le Roy, M. Jeletic, S. I. Gorelsky, I. Korobkov, L. Ungur, L. F. Chibotaru, M. Murugesu, *J. Am. Chem. Soc.* **2013**, *135*, 3502 – 3510; i) J. D. Rinehart, J. R. Long, *Chem. Sci.* **2011**, *2*, 2078 – 2085.

[11] a) S. Aime, M. Botta, E. Terreno, *Adv. Inorg. Chem.* **2005**, *57*, 173 – 237; b) P. Caravan, *Chem. Soc. Rev.* **2006**, *35*, 512 – 523; c) A. Datta, K. N. Raymond, *Acc. Chem. Res.* **2009**, *42*, 938 – 947; d) P. Hermann, J. Kotek, V. Kubicek, I. Lukes, *Dalton Trans.* **2008**, 3027 – 3047; e) J. Lee, M. J. Zylka, D. J. Anderson, J. E. Burdette, T. K. Woodruff, T. J. Meade, *J. Am. Chem. Soc.* **2005**, *127*, 13164 – 13166; f) E. C. Wiener, M. W. Brechbiel, H. Brothers, R. L. Magin, O. A. Gansow, D. A. Tomalia, P. C. Lauterbur, *Magn. Reson. Med.* **1994**, *31*, 1 – 8; g) C.-T. Yang, P. Chandrasekharan, T. He, Z. Poh, A. Raju, K.-H. Chuang, E. G. Robins, *Biomaterials* **2014**, *35*, 327 – 336.

[12] a) A. Martorana, G. Bellapadrona, A. Feintuch, E. Di Gregorio, S. Aime, D. Goldfarb, *J. Am. Chem. Soc.* **2014**, *136*, 13458 – 13465; b) A. M. Raitsimring, C. Gunanathan, A. Potapov, I. Efremenko, J. M. L. Martin, D. Milstein, D. Goldfarb, *J. Am. Chem. Soc.* **2007**, *129*, 14138 – 14139.

[13] a) B. Corzilius, A. A. Smith, A. B. Barnes, C. Luchinat, I. Bertini, R. G. Griffin, *J. Am. Chem. Soc.* **2011**, *133*, 5648 – 5651; b) J. W. Gordon, S. B. Fain, I. J. Rowland, *Magn. Reson. Med.* **2012**, *68*, 1949 – 1954.

[14] a) E. Colacio, J. Ruiz, G. Lorusso, E. K. Brechin, M. Evangelisti, *Chem. Commun.* **2013**, *49*, 3845 – 3847; b) I. A. Gass, E. K. Brechin, M. Evangelisti, *Polyhedron* **2013**, *52*, 1177 – 1180; c) T. N. Hooper, J. Schnack, S. Piligkos, M. Evangelisti, E. K. Brechin, *Angew. Chem. Int. Ed.* **2012**, *51*, 4633 – 4636; *Angew. Chem.* **2012**, *124*, 4711 – 4714; d) G. Lorusso, M. A. Palacios, G. S. Nichol, E. K. Brechin, O. Roubeau, M. Evangelisti, *Chem. Commun.* **2012**, *48*, 7592 – 7594; e) G. Lorusso, J. W. Sharples, E. Palacios, O. Roubeau, E. K. Brechin, R. Sessoli, A. Rossin, F. Tuna, E. J. L. McInnes, D. Collison, M. Evangelisti, *Adv. Mater.* **2013**, *25*, 4653 – 4656; f) V. K. Pecharsky, K. A. Gschneidner, Jr., *J. Magn. Magn. Mater.* **1999**, *200*, 44 – 56; g) A. M. Tishin, A. V. Derkach, Y. I. Spichkin, M. D. Kuz'min, A. S. Chernyshov, K. A. Gschneidner, V. K. Pecharsky, *J. Magn. Magn. Mater.* **2007**, *310*, 2800 – 2804; h) Y.-Z. Zheng, M. Evangelisti, F. Tuna, R. E. P. Winpenny, *J. Am. Chem. Soc.* **2012**, *134*, 1057 – 1065.

[15] R. D. McMichael, R. D. Shull, L. J. Swartzendruber, L. H. Bennett, R. E. Watson, *J. Magn. Magn. Mater.* **1992**, *111*, 29 – 33.

[16] M. Evangelisti, O. Roubeau, E. Palacios, A. Camon, T. N. Hooper, E. K. Brechin, J. J. Alonso, *Angew. Chem. Int. Ed.* **2011**, *50*, 6606 – 6609; *Angew. Chem.* **2011**, *123*, 6736 – 6739.

[17] a) G. Asgedom, A. Sreedhara, J. Kivikoski, J. Valkonen, E. Kolehmainen, C. P. Rao, *Inorg. Chem.* **1996**, *35*, 5674 – 5683; b) D. F. Back, C. R. Kopp, G. Manzoni de Oliveira, P. C. Piquini, *Polyhedron* **2012**, *36*, 21 – 29; c) V. Chandrasekhar, A. Dey, A. J. Mota, E. Colacio, *Inorg. Chem.* **2013**, *52*, 4554 – 4561; d) F.-S. Guo, J.-L. Liu, J.-D. Leng, Z.-S. Meng, Z.-J. Lin, M.-L. Tong, S. Gao, L. Ungur, L. F. Chibotaru, *Chem. Eur. J.* **2011**, *17*, 2458 – 2466; e) C. P. Rao, A. Sreedhara, P. V. Rao, M. B. Verghese, K. Rissanen, E. Kolehmainen, N. K. Lokanath, M. A. Sridhar, J. S. Prasad, *J. Chem. Soc. Dalton Trans.* **1998**, 2383 – 2394; f) Y. Sui, X. Zeng, X. Fang, X. Fu, Y. a. Xiao, L. Chen, M. Li, S. Cheng, *J. Mol. Catal. A* **2007**, *270*, 61 – 67; g) X. Zhang, P. Wei, J. Dou, B. Li, B. Hu, *Acta Crystallogr. Sect. E* **2009**, *65*, m293 – m294; h) Y. Guo, L. Li, Y. Liu, J. Dong, D. Wang, *Acta Crystallogr. Sect. E* **2008**, *64*, m675 – m676; i) D. Liu, Q. Zhou, Y. Chen, F. Yang, Y. Yu, Z. Shi, S. Feng, *Dalton Trans.* **2010**, *39*, 5504 – 5508; j) W. Zhu, S. Zhang, C. Cui, F. Bi, H. Ke, G. Xie, S. Chen, *Inorg. Chem. Commun.* **2014**, *46*, 315 – 319; k) E. Halevas, O. Tsave, M. P. Yavropoulou, A. Hatzidimitriou, J. G. Yovos, V. Psycharis, C. Gabriel, A. Salifoglou, *J. Inorg. Biochem.* **2015**, *147*, 99 – 115; l) H. Ke, L. Zhao, Y. Guo, J. Tang, *Dalton Trans.* **2012**, *41*, 9760 – 9765; m) H. Ke, L. Zhao, Y. Guo, J. Tang, *Dalton Trans.* **2012**, *41*, 2314 – 2319; n) H. S. Ke, Y. Guo, L. Zhao, J. K. Tang, *Sci. China Chem.* **2012**, *55*, 906 – 909; o) G. Wu, I. J. Hewitt, S. Mameri, Y. Lan, R. Clerac, C. E. Anson, S. Qiu, A. K. Powell, *Inorg. Chem.* **2007**, *46*, 7229 – 7231; p) R. Bircher, B. F. Abrahams, H. U. Guedel, C. Boskovic, *Polyhedron* **2007**, *26*, 3023 – 3028; q) H. Ke, L. Zhao, G.-F. Xu, Y.-N. Guo, J. Tang, X.-Y. Zhang, H.-J. Zhang, *Dalton Trans.* **2009**, 10609 – 10613; r) H. Ke, G.-F. Xu, L. Zhao, J. Tang, X.-Y. Zhang, H.-J. Zhang, *Chem. Eur. J.* **2009**, *15*, 10335 – 10338; s) S. Xue, L. Zhao, Y.-N. Guo, X.-H. Chen, J. Tang, *Chem. Commun.* **2012**, *48*, 7031 – 7033; t) S. Xue, L. Zhao, Y.-N. Guo, J. Tang, *Dalton Trans.* **2012**, *41*, 351 – 353; u) H.-H. Zou, L.-B. Sheng, Z.-L. Chen, F.-P. Liang, *Polyhedron* **2015**, *88*, 110 – 115.

[18] I. D. Brown, K. K. Wu, *Acta Crystallogr. Sect. B* **1976**, *32*, 1957 – 1959.

[19] a) H. Zabrodsky, S. Peleg, D. Avnir, *J. Am. Chem. Soc.* **1992**, *114*, 7843 – 7851; b) H. Zabrodsky, S. Peleg, D. Avnir, *J. Am. Chem. Soc.* **1993**, *115*, 8278 – 8289.

[20] a) P.-H. Lin, I. Korobkov, W. Wernsdorfer, L. Ungur, L. F. Chibotaru, M. Murugesu, *Eur. J. Inorg. Chem.* **2011**, 1535 – 1539; b) N. M. Randell, M. U. Anwar, M. W. Drover, L. N. Dawe, L. K. Thompson, *Inorg. Chem.* **2013**, *52*, 6731 – 6742; c) A. Wai-Hing Lam, W.-T. Wong, G. Wen, X.-X. Zhang, S. Gao, *New J. Chem.* **2001**, *25*, 531 – 533.

[21] M. U. Anwar, L. K. Thompson, L. N. Dawe, F. Habib, M. Murugesu, *Chem. Commun.* **2012**, *48*, 4576 – 4578.

[22] N. F. Chilton, R. P. Anderson, L. D. Turner, A. Soncini, K. S. Murray, *J. Comput. Chem.* **2013**, *34*, 1164 – 1175.

[23] D. N. Woodruff, F. Tuna, M. Bodensteiner, R. E. P. Winpenny, R. A. Layfield, *Organometallics* **2013**, *32*, 1224 – 1229.

[24] a) J. M. Zadrozny, M. Atanasov, A. M. Bryan, C.-Y. Lin, B. D. Rekken, P. P. Power, F. Neese, J. R. Long, *Chem. Sci.* **2013**, *4*, 125 – 138; b) A. Arauzo, A. Lazarescu, S. Shova, E. Bartolome, R. Cases, J. Luzon, J. Bartolome, C. Turta, *Dalton Trans.* **2014**, *43*, 12342 – 12356; c) S. M. J. Aubin, Z. Sun, L. Pardi, J. Krzystek, K. Folting, L.-C. Brunel, A. L. Rheingold, G. Christou, D. N. Hendrickson, *Inorg. Chem.* **1999**, *38*, 5329 – 5340; d) Y.-N. Guo, G.-F. Xu, P. Gamez, L. Zhao, S.-Y. Lin, R. Deng, J. Tang, H.-J. Zhang, *J. Am. Chem. Soc.* **2010**, *132*, 8538 – 8539; e) Y.-N. Guo, G.-F. Xu, W. Wernsdorfer, L. Ungur, Y. Guo, J. Tang, H.-J. Zhang, L. F. Chibotaru, A. K. Powell, *J. Am. Chem. Soc.* **2011**, *133*, 11948 – 11951; f) P.-H. Lin, T. J. Burchell, L. Ungur, L. F. Chibotaru, W. Wernsdorfer, M. Murugesu, *Angew. Chem. Int. Ed.* **2009**, *48*, 9489 – 9492; *Angew. Chem.* **2009**, *121*, 9653 – 9656.

[25] a) E. Lucaccini, L. Sorace, M. Perfetti, J.-P. Costes, R. Sessoli, *Chem. Commun.* **2014**, *50*, 1648 – 1651; b) P.-E. Car, M. Perfetti, M. Mannini, A. Favre, A. Caneschi, R. Sessoli, *Chem. Commun.* **2011**, *47*, 3751 – 3753;

c) M. Perfetti, E. Lucaccini, L. Sorace, J. P. Costes, R. Sessoli, *Inorg. Chem.* **2015**, *54*, 3090 – 3092.

[26] a) L. Ungur, M. Thewissen, J.-P. Costes, W. Wernsdorfer, L. F. Chibotaru, *Inorg. Chem.* **2013**, *52*, 6328 – 6337; b) L. Ungur, L. F. Chibotaru, *Phys. Chem. Chem. Phys.* **2011**, *13*, 20086 – 20090.

[27] L. F. Chibotaru, L. Ungur, *J. Chem. Phys.* **2012**, *137*, 064112/064111 – 064112/064122.

[28] R. A. Layfield, M. Murugesu, L. Ungur, L. F. Chibotaru, in *Lanthanides and Actinides in Molecular Magnetism*, Wiley-VCH, Weinheim, **2015**, pp. 153 – 184.

[29] R. Orbach, *Proc. R. Soc. London Ser. A* **1961**, *264*, 485 – 495.

[30] a) S. K. Singh, T. Gupta, M. Shanmugam, G. Rajaraman, *Chem. Commun.* **2014**, *50*, 15513 – 15516; b) C. Das, A. Upadhyay, S. Vaidya, S. K. Singh, G. Rajaraman, M. Shanmugam, *Chem. Commun.* **2015**, *51*, 6137 – 6140; c) P. Zhang, L. Zhang, C. Wang, S. Xue, S.-Y. Lin, J. Tang, *J. Am. Chem. Soc.* **2014**, *136*, 4484 – 4487.

[31] S. K. Langley, D. P. Wielechowski, V. Vieru, N. F. Chilton, B. Moubaraki, L. F. Chibotaru, K. S. Murray, *Chem. Sci.* **2014**, *5*, 3246 – 3256.

[32] N. F. Chilton, D. Collison, E. J. L. McInnes, R. E. P. Winpenny, A. Soncini, *Nat. Commun.* **2013**, *4*, 2551.

[33] P.-H. Guo, J.-L. Liu, Z.-M. Zhang, L. Ungur, L. F. Chibotaru, J.-D. Leng, F.-S. Guo, M.-L. Tong, *Inorg. Chem.* **2012**, *51*, 1233 – 1235.

[34] S. K. Langley, D. P. Wielechowski, V. Vieru, N. F. Chilton, B. Moubaraki, B. F. Abrahams, L. F. Chibotaru, K. S. Murray, *Angew. Chem. Int. Ed.* **2013**, *52*, 12014 – 12019; *Angew. Chem.* **2013**, *125*, 12236 – 12241.

[35] A. Bhunia, M. T. Gamer, L. Ungur, L. F. Chibotaru, A. K. Powell, Y. Lan, P. W. Roesky, F. Menges, C. Riehn, G. Niedner-Schatteburg, *Inorg. Chem.* **2012**, *51*, 9589 – 9597.

[36] L. Ungur, S. K. Langley, T. N. Hooper, B. Moubaraki, E. K. Brechin, K. S. Murray, L. F. Chibotaru, *J. Am. Chem. Soc.* **2012**, *134*, 18554 – 18557.

[37] a) S.-Y. Lin, W. Wernsdorfer, L. Ungur, A. K. Powell, Y.-N. Guo, J. Tang, L. Zhao, L. F. Chibotaru, H.-J. Zhang, *Angew. Chem. Int. Ed.* **2012**, *51*, 12767 – 12771; *Angew. Chem.* **2012**, *124*, 12939 – 12943; b) S. Xue, X.-H. Chen, L. Zhao, Y.-N. Guo, J. Tang, *Inorg. Chem.* **2012**, *51*, 13264 – 13270.

[38] M. Evangelisti, F. Luis, L. J. de Jongh, M. Affronte, *J. Mater. Chem.* **2006**, *16*, 2534 – 2549.

[39] Y.-Z. Zheng, M. Evangelisti, R. E. P. Winpenny, *Angew. Chem. Int. Ed.* **2011**, *50*, 3692 – 3695; *Angew. Chem.* **2011**, *123*, 3776 – 3779.

[40] a) S. K. Langley, N. F. Chilton, B. Moubaraki, T. Hooper, E. K. Brechin, M. Evangelisti, K. S. Murray, *Chem. Sci.* **2011**, *2*, 1166 – 1169; b) J.-B. Peng, Q.-C. Zhang, X.-J. Kong, Y.-Z. Zheng, Y.-P. Ren, L.-S. Long, R.-B. Huang, L.-S. Zheng, Z. Zheng, *J. Am. Chem. Soc.* **2012**, *134*, 3314 – 3317.

Received: July 10, 2015
Published online on September 18, 2015